Author Version of : Oceanologia, vol.63(2); 2021; 261-275

Response of coastal phytoplankton to upwelling induced hydrological changes in the Alappuzha mud bank region, southwest coast of India

Nikathithara Velappan Madhu*, Pearia Anil, Paul Meenu, Thundiyil Raju Gireeshkumar, Kallungal Ravunnikutty Muraleedharan, Thekkendavida Velloth Rehitha, Mathew Dayana, Chazhikulam Rajan Vishal

CSIR-National Institute of Oceanography, Regional Centre, Kochi-682018

*Corresponding Author:- nmadhu@nio.org

Abstract

The response of phytoplankton community to the co-existing events of coastal upwelling and mud banks in the nearshore waters of Alappuzha (15 m depth), located in the southwest coast of India from April to November 2016, is described based on size-fractionated phytoplankton biomass (chlorophyll *a*), primary production and community composition. The study region exhibited well-distinct spatio-temporal hydrological changes because of the influence of wind-driven coastal upwelling, prevalent during the southwest monsoon (SWM) period. However, the formation of mud banks, in addition to coastal upwelling, was observed at station M2, which facilitated the substantial increase of water column turbidity and inorganic nutrients (ammonium, phosphate, and silicate) during and after the peak SWM period compared to the non-mud bank reference stations (M1 and M3). The prevailing hydrological changes were complemented the corresponding phytoplankton productivity patterns, in which profound domination of nanophytoplankton (2 - 20 µm) chlorophyll *a* and primary production was observed throughout the study region, irrespective of seasons. The SIMPER analysis, based on phytoplankton (mostly >20 µm) species composition data (microscopy), revealed the formation of certain *characterizing species*, mainly comprised of diatoms and dinoflagellates. The consistent predominance of the nanophytoplankton, established under variable hydrological scenarios, showed that the inorganic nutrient (specifically ammonium) availability was instrumental in defining the widespread growth of nanophytoplankton community compared to the prevailing light levels. The present study thus revealed that even the small-sized phytoplankton community could survive in the nutrient-enriched coastal waters, characterised by the co-existing upwelling and mud banks.

Keywords:- Mudbank; Upwelling; Phytoplankton; Chlorophyll *a*; Algal bloom; Alappuzha

1. Introduction

Phytoplankton community in the coastal marine ecosystems habitually experiences a large-scale spatio-temporal variability in their biomass, productivity, species composition, abundance, and community structure due to the dynamic nature of the prevailing environmental conditions (Subrahmanyam, 1959; Sommer, 2012). Seasonally occurring natural (e.g., coastal upwelling, terrestrial runoff and river discharges) and anthropogenic perturbations (e.g., domestic and industrials waste disposal) lead to frequent nutrient-enrichments in the coastal waters and thus escalates significant phytoplankton growth and biomass accumulations (Pauly & Christensen, 1995). The coastal upwelling systems exhibit unique phytoplankton growth patterns and species successions corresponding to the various stages of upwelling (Lips and Lips, 2010). Larger phytoplankton (mostly >20 µm in size), mainly comprised of diatoms and dinoflagellates, seasonally flourish in the tropical coastal marine waters in response to the wind-driven upwelling induced nutrient enrichments (Wilkerson et al., 2000; Shangguan et al., 2017). Medium to large-sized phytoplankton prefer to grow in nitrate enriched coastal marine waters; mostly diatoms and dinoflagellates are recognized as the predominant phytoplankton taxa in this size category (Anabalon et al., 2007; Lips and Lips, 2010), and the dominance of this large-sized phytoplankton in coastal waters eventually lead to the preponderance of herbivorous trophic food web (Azam et al.,1983). On the other hand, small-sized phytoplankton (<20 µm), for example, small diatoms, dinoflagellates, cryptophytes, nano-eukaryotes, etc. and also picophytoplankton (<2µm, i.e., *Synechococcus, Prochlorococcus* and pico-eukaryotes) are reported to grow in oligotrophic tropical and subtropical waters where the microbial food web predominates (Azam et al., 1983; Calvo-Díaz et al., 2006; Agustí and Llabrés, 2007; Matsumoto et al., 2016). However, in contrast with the general understanding, recent reports have revealed that even small-sized phytoplankton can grow faster in the upwelled regions where ammonium dominates (Kuvaldina et al., 2010; Lips and Lips, 2010).

The mud banks or *Chakara* is a unique coastal oceanographic phenomenon that occurs in the nearshore waters of the southwest coast of India, particularly in the Kerala coast, in fragmented stretches of calm turbid waters along with considerably higher suspended sediments (Bristow, 1938; Silas 1984; Shynu et al., 2017). These mud banks, usually developed in the nearshore waters (<10 m depth) during the southwest monsoon (SMW hereafter) period either at or near river mouths, holding loads of terrigenous organic and inorganic materials in association with the torrential monsoonal rainfall and runoff (Silas, 1984; Qasim, 2003). However, the mud banks that occur in the Alappuzha coast (Figure 1a) are rather different from the usual mud banks of the Kerala coast because of the lack of river influence in its immediate vicinity (Kurup, 1972; Silas, 1984). Furthermore, all the mud banks

reported from the Alappuzha coast are unique in their physical appearance and biogeochemical processes (Silas, 1984; Jyothibabu et al., 2018b). The Alappuzha mud banks (AMBs hereafter), in general, appeared to be a semi-circular shaped shallow (~ 7 to 15 m depth) water body, extending up to approximately 8 km offshore (from the coast) and 3 to 4 km alongshore (Tatavarthi and Narayana, 2006; Muraleedharan et al., 2017). The characteristic colloidal fluid mud accumulation in the bottom layers of this specialized coastal ecosystem usually enables damping of high waves prevalent during the SWM period (Shynu et al., 2017; Samiksha et al., 2017), and eventually, it creates a calm and conducive environment for the smooth operation of fishing activities (Reghunathan et al., 1984; Silas, 1984). There are many reports delineating the physical (Silas 1984; Mallik et al., 1988; Balachandran, 2004; Tatavarthi and Narayana, 2006), chemical (Gireesh Kumar et al., 2017; Dayana et al., 2019) and biological (Mathew et al., 1984; Damodaran et al., 1972 and 1973; Reghunathan et al., 1984; Karnan et al., 2017; Jyothibabu et al., 2018a) properties of the AMBs for the last 3 to 4 decades. However, a valid reason for the recurrent mud bank formation in the Alappuzha coast (during the SWM period) is still unknown to the scientific world (Jyothibabu et al., 2018b). Even then, some of the reports have claimed a significant role of coastal upwelling on mud bank formation in the Alappuzha coast (Ramasastry and Myrland 1959; Philip et al., 2013; Muraleedharan et al., 2017). By assessing the physical appearance, it was reported that the AMBs usually start developing in the nearshore waters (~5 to 10 m depth) during the onset of SWM (June) (Muraleedharan et al., 2017). Subsequently, it persists in the region until the end of SWM (September) (Silas, 1984; Muraleedharan et al., 2017). Many of the recent studies have elucidated the upwelling induced physico-chemical (Muraleedharan et al., 2017; Gireesh Kumar et al., 2017; Dayana et al., 2019) and biological (Jagadeesan et al., 2017; Karnan et al., 2017; Jyothibabu et al. 2018a and 2018b) changes of AMBs using a comprehensive set of time-series data collected during 2014.

Even though a large number of studies have been carried out for the last few decades to delineate the physico-chemical characteristics (Kurup, 1972; Silas 1984; Tatavarthi and Narayana, 2006; Muraleedharan et al., 2017; Dayana et al., 2019), an appropriate interpretation of phytoplankton dynamics, specifically the size-structure based productivity pattern, was not made so far. Even then, some of the recent studies have thoroughly elucidated various ecological aspects of the plankton community using state-of-the-art analytical techniques and procedures (Jagadeesan et al., 2017; Karnan et al., 2017; Jyothibabu et al. 2018a and 2018b). As far as the phytoplankton community is concerned, its cell size has been recognized as a morphological parameter of prime physiological and ecological significance (Malone, 1980; Raven, 1986). Therefore, the size-structure based productivity studies have a vital role in understanding the pelagic food web structure of a coastal water ecosystem

(Fenchel, 1988). The phytoplankton community has been typically categorized into pico- (<2 µm), nano- (2-20 µm), and micro-phytoplankton (20-200 µm) groups based on their cell size (Sieburth et al., 1978). According to recent reports, the AMBs sustained significantly high phytoplankton biomass in terms of chlorophyll *a*, derived mostly from large-sized (>20 µm) phytoplankton, mainly comprised of diatoms and dinoflagellates (Karnan et al., 2017; Jyothibabu et al., 2018a). Furthermore, the AMB region has been recognized for the frequent formation of various algal blooms (Jyothibabu et al., 2018b; Madhu et al., 2020) due to the upwelling induced seasonal nutrient enrichments (Gireesh Kumar et al., 2018; Dayana et al., 2019). Considering all the aspects mentioned above, the present study aims to elucidate (1) the overall phytoplankton productivity patterns of the Alappuzha nearshore waters, including the mud bank region on a spatio-temporal scale, (2) the productivity (chlorophyll *a* and primary productivity) contributions of various phytoplankton size-groups and (3) the community composition and species successions.

2.Materials and Methods

2.1.Study area and sampling strategy

The present study was formulated on the basis of time-series (weekly/biweekly/monthly) field observations carried out in three pre-fixed stations (M1, M2 and M3), in the nearshore waters (<15 m depth) of Alappuzha, located in the southwest coast of India, including the mud bank region (Figure 1a). The field samplings were conducted from April 2016 to November 2016 using a mechanized powerboat. A total of 16 observations were carried out in the study region during the whole study period. The sampling station M1 was located ~7 km away northward from the mud bank region, at a depth of ~ 6 m. The second station M2, was fixed inside the mud bank region (<6 m depth), wherein a conspicuous mud accumulation was physically evident by the occurrence of calm sea surface between mid-June and September end (Muraleedharan et al., 2017). The third station M3, was located in the offshore boundary of the mud bank region, perpendicular to station M2 at a depth of 12 to 13 m. During the Pr.SWM period, the AMB region (M2) was appeared to be warm with a clear atmosphere and high waves (>1 m) (Figure 1b); cloudy sky (due to the monsoonal rainfall) with calm and turbid waters during the SWM period (Figure 1c); warm sunny atmosphere along with a calm, less turbid waters during the Pt.SWM period (Figure 1d).

2.2.Sampling and analytical methods

The major meteorological parameters such as wind speed and rainfall (daily basis) were retrieved from the online site of Physical Sciences Division of Earth System Research Laboratory, NOAA (https://www.esrl.noaa.gov/psd/data/gridded/data.ncep.reanalysis.html) and Indian

Meteorological Department (IMD). A portable CTD (SBE, Seabird Electronics, USA) comprised of appropriate sensors was used to retrieve the vertical profiles of the water column temperature, salinity, turbidity and PAR (photosynthetically active radiation). The water samples for chemical and biological parameters were collected from the near-surface (0.5 m), mid-depth, and near-bottom waters using an acid cleaned 5-L PVC Niskin bottles equipped with Teflon-coated springs. The collected water samples were immediately transferred to an acid cleaned polyethylene bottles, kept on ice boxes filled with ice, and brought to the laboratory for further analysis. The concentration of dissolved oxygen (DO) was estimated by Winkler's method using an automatic titration system (Metrohm 865 Dosimat plus), following Grasshoff et al, (1983). The major inorganic nutrients such as ammonium (NH_4^+), nitrate (NO_3^-), phosphate (PO_4^{3-}), and silicate (SiO_4) were analyzed using a calibrated autoanalyzer (Skalar San^{++}).

The estimation of size-fractionated phytoplankton biomass (chlorophyll *a*) was carried out by the sequential filtering of 1 L water sample from desired depths, initially through 20 μm nylon sieve and subsequently through 2 and 0.2 μm cellulose nitrate filters. The cells retained by the 20 μm sieve are designated as microphytoplankton (>20 μm), which later concentrating on Whatman GF/F filters (nominal pore size 0.7 μm), whereas those retained by 2 and 0.2 μm filters taken as the nano- (2 to 20 μm) and pico- (<2 μm) phytoplankton size category, respectively. After filtration, the filters containing phytoplankton were extracted in 90% acetone after keeping in the dark (18 to 24 hours) at 4°C and chlorophyll *a* was estimated fluorometrically (Fluorometer, Model-7200, Turner). Similarly, the size-fractionated primary production was determined by running '*simulated in-situ*' incubations with the isotope ^{14}C. Four 300-ml acid-washed biological oxygen demand glass bottles (three-light and one dark bottle) were filled with water collected from various depths. Each bottle was inoculated with 1 ml 5 μCi $NaH^{14}CO_3$ and incubated for 6 hr (12 pm - 6 pm). At the end of incubations, samples were sequentially filtered through 20-μm nylon mesh and 2- and 0.2 μm polycarbonate filters. The phytoplankton cells concentrated in the 20 μm mesh were washed with filtered (through 0.2 polycarbonate filters) seawater and again concentrated on GF/F filters (nominal pore size - 0.7 μm). After the treatment with concentrated hydrochloric acid fumes to remove inorganic carbon, the filters were analyzed in the Liquid scintillation counter (Perkin Elmer-Liquid Scintillation Analyzer, Tri carb 2810 TR). The primary production rate was calculated according to the equation described in the protocol (Parsons et al., 1984). For the qualitative and quantitative studies of phytoplankton, 1 L of water sample was taken from the near-surface waters and fixed with acid Lugol's iodine solution. After the settling and siphoning procedure following Utermöhl (1958), 1 ml of an aliquot of the sample was taken in a Sedgewick-Rafter counting cell in duplicate for enumeration of cells under the inverted

binocular microscope (Olympus CK30), following standard identification manuals (Tomas, 1997; Subrahmaniam, 1959).

2.3. Data analysis

To understand the spatio-temporal variability in phytoplankton species assemblages, a statistical software PRIMER version 6 (Clarke and Gorley, 2015) was adopted to calculate the species diversity index (*H'*). The identification of *characterizing* species was accomplished using the similarity percentage routine (SIMPER) analysis using the 4^{th} root-transformed species abundance data described in PRIMER version 6. The redundancy analysis (RDA) was performed to elucidate the inter-relationships existing between the abiotic and biotic variables, especially the critical environmental factors controlling the distribution of the phytoplankton community. For this, the abiotic variables included were temperature, salinity, PAR, turbidity, and inorganic nutrients, while for the biotic variables, the data on biomass (chlorophyll *a*) and primary productivity of various phytoplankton size-groups (pico-, nano- and micro-) and also species abundance were included.

3. Results

3.1. Physico-chemical properties

Generally, the whole study region was experienced with relatively weak winds (<5 m s^{-1}) during the Pr.SWM (April-May) and Pt.SWM (October-November) periods (Figure 2). Conversely, slightly strong winds (6 - 7m s^{-1}) were prevalent during the onset of SWM as a part of the prevailing southwesterly (Smitha et al., 2014). The recorded rainfall over the study region was apparently high (av. 7.7 ± 5.8 mm d^{-1}) during the SWM period, with a distinct peak observed in June (av. 15.1 ± 5.8 mm d^{-1}) (Figure 2). The upper water column of the whole study region was prominently warm (>31°C) and well mixed during the Pr.SWM period (Figures 3a-c). However, a gradual drop in surface water temperature (~3°C) was evident from May end to mid-June. Later, a marked decrease (up to 25°C) in water column temperature (even on the surface) was detected at all three sampling stations, along with signatures of thermal stratification (Figure 3a-c). The lowest water column temperature (<25°C) was perceived during the peak SWM (July to September beginning), more evidently at station M3 (Figures 3a-c). In the beginning of October (Pt.SWM), a drastic rise in water column temperature (26 - 30°C) was detected in the study region and it sustained even warmer (>31°C) and well mixed till November. The water column salinity also showed a distinct temporal scale variation, wherein relatively high salinity (>34) was observed during the Pr.SWM and Pt.SWM periods (Figures 3d-f). An intermittent salinity drop (<34 plumes) were detected during the peak SWM period over the whole study region, particularly at M1 and M2.

The water column turbidity apparently showed a distinctive spatio-temporal variation over the whole study region (Figures 3 g-i). The station M2 sustained high levels of water column turbidity (12-20 NTU) compared to M1 and M3, especially during the SWM period (Figures 3 g-i). At station M2, a gradual increase in water column turbidity (8 - 20 NTU) was detected since the beginning of June, and it gets persisted at the subsurface layers until late July (~4 m depth). The PAR level, in general, was consistently high (>200 µ mol photon m^{-2} d^{-1}) in the water column (above 4 m depth) of station M3 (Figures 3 j-l). By contrast, high PAR (>200 µ mol photon m^{-2} d^{-1}) was restricted only in the surface layers (1-2 m depth) at stations M1 and M2.

The prevalence of moderate oxygenated (>150 µM) water column was evident over the study region during the Pr.SWM period and this condition found sustain until the onset of SWM (Figures. 4a - c). Later, the whole study region exhibited pronounced hypoxic (≤ 65 µM) waters approximately below 3 m depth. At station M3, this oxygen deficiency period extended a little longer (July to late September), indicated the prevalence of comparatively stronger coastal upwelling than that experienced at M1 and M2. The distribution of inorganic nutrients (e.g., NH_4^+, NO_3^-, PO_4^{3-} and SiO_4) exhibited a distinctive spatio-temporal variation (Figures 4d-o). Exceptionally higher levels of NH_4^+, PO_4^{3-} and SiO_4 recorded at all three stations (specifically at M2) during the complete span of SWM. The dissolved inorganic nitrogen (DIN) was primarily constituted by NH_4^+ (> 80 %) in all three sampling stations, irrespective of seasons (Figures 4d - f). However, a noticeable increase in NH_4^+ (>10 µM) was detected during the SWM period (since June 3rd week), particularly at M2 (Table 1). A noticeable increase in PO_4^{3-} (>1 µM) and SiO_3 (>18 µM) were also perceived at all three stations during the SWM period along with NH_4^+ (Figures 4j-o). The station M2 sustained high levels PO_4^{3-} and SiO_3 till the end of the SWM period (September). By contrast, NO_3^- in general, remained apparently low (<1 µM) at all three stations during the pre-/post-phases of SWM (Figures 4 g-i). However, a slight increase in NO_3^- was observed throughout the study region during the SWM period (since 14th June). This NO_3^- enrichment was specifically discernible at M3, wherein a progressive increase in NO_3^- was detected since June 1st week. The nutrient ratios, mainly N:P and N:Si, showed high values because of the prevalence of consistently high DIN, which was primarily enabled by NH_4^+ (Table 1). During the Pr.SWM period, the whole study region was characterized by slightly high N:Si ratios (>2) because of the prevalence of low silicate (<5 µM) in the water column. The pronounced decrease in NO_3^- to PO_4^{3-} ratios (<3) apparent in the whole study region indicated NO_3^- deficiency, especially on the surface, regardless of seasons.

3.2. Size-fractionated phytoplankton chlorophyll a

Corresponding to the conspicuous seasonal heterogeneity in the distribution of hydro-physical/chemical properties, the phytoplankton chlorophyll *a* (chl *a* hereafter) also showed a remarkable spatio-temporal variation both in the surface (Figures 5a-c) and water column (Figures 7a-c). The intense blooming of an autotrophic small-sized (<25 µm) dinoflagellate species causes an exceptionally high chl *a* at the surface (22.84 mg m^{-3}) and water column (108.6 mg m^{-2}) of station M2 during the peak SWM period, specifically on 7 September (Figure 5b). The size-fractionated biomass estimations have shown the significant contribution of chl *a* (70-90 %) from the nanophytoplankton community, irrespective of seasons. During the Pr.SWM period, although stations M1 and M2 sustained relatively high chl *a* (>4 mg m^{-3}), derived from nanophytoplankton, station M3 remained low levels of chl *a* (< 1 mg m^{-3}) (Figure 5). However, during the onset of SWM, relatively low levels of chl *a* (<1 mg m^{-3}) was evident at M1 and M2, indicating the prevalence of oligotrophic condition (Figure 5). At station M3, a subsurface chl *a* peak was discernible (16.16 mg m^{-3}) during this period, indicated the combined contribution of both nanophytoplankton (11.39 mg m^{-3}) and microphytoplankton (4.68 mg m^{-3}) communities. A consistently low levels of chl *a* (<0.2 mg m^{-3}) from picophytoplankton (<2 µm) community was obvious in the whole study region, irrespective of seasons, which signifies the prevalence of exceptionally low abundance of picophytoplankton (Figures 5j-l).

3.3. Size-fractionated primary production

The results of primary production (PP hereafter) estimations using simulated *in-situ* (deck incubation) ^{14}C method showed more or less similar distribution patterns of chl *a* (Figures 6a-c). The total PP in the surface waters was relatively high at stations M1 and M2, whereas as the column PP was obviously high at M3 (because of deeper photic depth), especially during the SWM period (Figures. 8 d-f). Clear-cut domination of nanophytoplankton PP was evident in the whole study region compared to the production rates of pico- and microphytoplankton communities (Figures 7d-l). On a seasonal scale, station M2 sustained high surface PP (> 250 mg C $m^{-3}d^{-1}$) during the SWM period. During the peak SWM, a substantial increase in PP both in surface (2438 mg C m^{-3} d^{-1}) and water column (8453 mg C m^{-2} d^{-1}) of station M2 was recorded, which was found to be complemented the chl *a* increase enabled by the dinoflagellate bloom (Figure 5b). Generally, microphytoplankton PP rates also greatly varied spatio-temporally similar to nanophytoplankton. Station M3 exhibited relatively high PP rates from microphytoplankton community compared to M1 and M2. The picophytoplankton PP showed a widespread decrease (<10 mg C m^{-3} d^{-1}) across the study region throughout the sampling period similar to chl *a* levels; however, a small-scale increase (>15 mg C m^{-3} d^{-1}) was evident at M2 during the SWM period (Figure 5 & 6).

3.4. Phytoplankton abundance, composition and *diversity*

The microscopy-based phytoplankton species composition (mostly >20 µm size) and numerical abundance in the surface waters showed an apparent spatio-temporal variation in the study region owing to the proliferation of certain diatoms and dinoflagellates (Figure 8). The total phytoplankton abundance was seemingly high at M1 and M2 compared to M3, and the overall community was mostly comprised of diatoms. However, an intermittent dominance of certain dinoflagellate species (even as blooms) was also detected during the SWM period, especially at station M2. The overall phytoplankton abundance varied between 0.1 x 10^3 cells L^{-1} and 14679.25 x 10^3 cells L^{-1} all through the sampling period. The proliferation of a centric diatom, *Trieres mobiliensis* (138.6 x 10^3 cells L^{-1}), was detected at M1 during the Pr.SWM period (4^{th} April). Similarly, an intense bloom (brownish discolouration) of a small-sized (<25 µm) autotrophic dinoflagellate, *Prorocentrum shikokuense* Hada (14664 x 10^3 cells L^{-1}) was also detected at M2 during the peak SWM period (7^{th} September 2016). The seasonal scale phytoplankton species diversity index (*H'*) was slightly high at M1 (av.3.99 ± 0.58) and M2 (av.3.85 ± 0.59) compared to M3 (av.3.65 ± 0.51). The results of SIMPER analysis have brought out ample information on *characterizing species* for each station with a wide temporal scale similarity (22.86 - 43.49%), which was mainly comprised of relatively larger (>20 µm) diatoms and dinoflagellates (Figure 9). The *characterizing species* also showed a distinctive spatio-temporal variation in their occurrence and relative abundance. Majority of the *characterizing species* for each station was formed of both diatoms (e.g., *Cosciodiscus* sp., *Trieres mobiliensis*, *Pleurosigma* sp., *Thalassiosira* sp., *Chaetoceros* sp., *Rhizosolenia hebetata*, *Pseudo-nitzschia* sp., *Navicula* sp.) and dinoflagellates (e.g., *Tripos furca*, *Dinophysis caudata*, *Prorocentrum micans*, *Tripos muelleri*, *Protoperidinium* sp., *Diplosalis* sp.). *Tripos furca* and *Coscinodiscus* sp. invariably performed as the predominant *characterizing species* to all three stations, during the Pr.SWM and SWM periods. Similarly, *Trieres mobiliensis* and *Dinophysis caudata* were identified as the major *characterizing species* of stations M1 and M2 during the Pr.SWM period.

3.5. Redundancy analysis

The influence of prevailing environmental factors on the size-structure based phytoplankton productivity (chl *a* and PP) was explored using the redundancy analysis (RDA). The overall phytoplankton productivity, in particular, nanophytoplankton chl *a* and PP, was found to be influenced by NH_4^+, PO_4^{3-} and SiO_4, specifically for station M2 because of the significant positive correlation (Figure 10a). By contrast, sea surface temperature and salinity were the major influencing factors of phytoplankton productivity for stations M3 (throughout) and M1 (mostly during the pre-/post SWM periods). The RDA plot, depicting the interrelationships between the environmental parameters and

phytoplankton *characterizing species* (derived by SIMPER analysis), revealed the significant influence of turbidity and temperature towards certain diatoms (e.g.,*Trieres mobiliensis* and *Chaetoceros* sp.) and dinoflagellates (e.g.,*Tripos furca, Prorocentrum micans, Protoperidinium* sp., and *Gonyaulax* sp.) of larger size (>20 µm), evident mostly during the pre-and post SWM periods regardless of stations. On the other hand, during the SWM period, the most of the *characterizing species* (e.g., *Thalassiosira subtilis, Coscinodiscus* sp., *Rhizosolenia hebetate, Odontella* sp., *Pleurosigma* sp., *Navicula* sp., *Pseudo-nitzschia seriata*., *Dinophysis caudata* and *Diplosalis* sp.) were found to be influenced by a suite of environmental parameters (Salinity, DO,PAR, PO_4^{3-}, SiO_3 and NO_3) shown in figure 10b.

4. Discussion

The coastal marine waters in and around the AMB region usually sustain high inorganic nutrients during the SWM period (Silas, 1984; Gireesh kumar et al., 2017; Dayana et al., 2019), which was reported to be brought by the wind-driven coastal upwelling prevalent in the nearshore waters of southeastern Arabian Sea (SEAS) (Hareesh Kumar et al., 2009; Muraleedharan et al., 2017). The upward transport of nutrient-rich bottom waters eventually activates phytoplankton growth in surface waters, leading to large-scale biomass (chl *a*) accumulation (Banse, 1959; Habeebrehman et al., 2008; Jyothibabu et al., 2010). The overall biogeochemical manifestations established in the nearshore waters of SEAS, in connection with the coastal upwelling and monsoon-driven freshwater influx, found to be persisted between June and September months, or sometimes it may be extended to late October (Banse, 1959; Habeebrehman et al., 2008). During this period, the whole nearshore waters of SEAS experiences various biogeochemical anomalies, including formation of hypoxia (Naqvi et al., 1994; Gireesh kumar et al., 2017), algal blooms (Subrahmaniam, 1959; Sahayak et al., 2005; Padmakumar et al., 2010a; Karnan et al., 2017; Jyothibabu et al., 2018b; Madhu et al., 2020), zooplankton swarming (Nair et al., 1992; Jagadeesan et al., 2017), high fish abundance (Banse 1959; Reghunathan et al., 1984), etc. Usually, widespread dominance of diverse diatom species occurs in this region during the SWM period (Subrahmanyam 1959; Banse, 1959). However, this diatom preponderance was sometimes replaced by certain dinoflagellates belonging to both autotrophic (e.g.,*Prorocentrum shikokuense*, *Karenia mikimotoi*) and heterotrophic (e.g., *Noctiluca scintillans*) species as blooms (red tide), mainly during the waning phase of SWM (September) (Subrahmanyam, 1959, Nair et al., 1992; Sahayak et al., 2005; Padmakumar et al., 2010a; Madhu et al., 2011). Usually, the upwelling zones are characterized by the abundance of larger phytoplankton (mainly diatoms) because of their effective utilization capacity of the surplus inorganic nutrients, especially NO_3^-, in the water column (Stolte et al., 1994; Lassiter et al., 2006; Anabalon et al., 2007). Such scenarios were documented in the

nearshore waters of SEAS as well during the SWM period (Subrahmanyam, 1959; Nair et al., 1992; Karnan et al., 2017). However, reports from temperate upwelling waters showed a faster growth response of smaller phytoplankton (<20 μm) in the upwelled region enriched with NH_4^+ (Kuvaldina et al.,2010; Lips and Lips 2010).

The progressive changes in hydrological properties evident all along the Alappuzha nearshore waters during the present study was found to be mainly governed by the coastal upwelling and related environmental perturbations (Silas 1984; Muraleedharan et al., 2017; Gireesh kumar et al., 2018). The apparent warm (>31 ºC), oxygenated (>200 μM), and nutrient-depleted (specifically NO_3^- and PO_4^{3-}) waters prevalent during the Pr.SWM period indicated the typical oligotrophic condition of the SEAS (Bhattathiri et al., 1998; Madhu, 2005; Jyothibabu et al., 2010). However, a noticeable increase in NH_4^+ (<5 μM) and SiO_4 (<3 μM) observed across the shallow stations (M1 and M2) in April/May months showed the terrestrial influence because of its proximity (Figure 4). Similarly, the occurrence of subsurface cold water (<29°C) detected all along the coast during the onset of SWM (June) indicates the early signatures of coastal upwelling. Subsequently, by the end of June, the whole study region gets transformed into a typical cold (<27°C) water dominated zone as a result of the advection of upwelled waters by the influence of prevailing coastal currents (Muraleedharan et al., 2017). However, the presence of prominent cold waters (25°C) observed in the surface layers of station M3 by the end of June implied that the upwelling process might have initiated at this station a little early because of its deeper depth (Hareesh Kumar et al., 2009; Smitha et al., 2014; Muraleedharan et al., 2017). A noticeable increase in water column turbidity observed exclusively at M2 obviously showed the formation of mud banks during the SWM monsoon period (specifically between 8th June and 8th August); substantiated by the prevalence of calm sea surface devoid of waves (Shynu et al., 2017; Muraleedharan et al., 2017). The inorganic nutrients, particularly NH_4^+, PO_4^{3-} and SiO_4 were relatively high in all three stations during the SWM period (Figure 4). However, NO_3^- levels (< 2 μM) were apparently low throughout the study region, especially at stations M1 and M2 (Figure. 4). According to previous reports, the AMB region sustained high levels of NO_3^- (>7μM) during the SWM period owing to the influence of intense coastal upwelling (Gireeshkumar et al., 2017; Dayana et al., 2019). By contrast, the prevalence of low NO_3^- levels at stations M1 and M2 signifies week upwelling compared to the upwelling that occurred at station M3. Recently, Dayana et al, (2019) have reported a significant role of fluid mud in the AMB region in supplementing some of the major inorganic nutrients (i.e., NH_4^+, PO_4^{3-} and SiO_4) in the water column during the peak SWM period.

The tropical coastal marine environments, in general, are expected to be highly productive (specifically phytoplankton growth), regardless of seasons, as a result of the high nutrient inputs from

various sources (Estrada et al., 2016). However, the nearshore waters of SEAS usually exhibit a distinct seasonality in phytoplankton growth (Bhattathiri et al., 1996; Madhu, 2005; Habeebrehman et al., 2008) because of the prevailing spatio-temporal variation in inorganic nutrients (Jyothibabu et al., 2010; Vijay et al., 2014). The SEAS, in general, found to be warm and nutrient-depleted during the Pr.SWM period, which, in turn, leads to the prevalence of low phytoplankton productivity (Jyothibabu et al., 2010; Madhu et al., 2017). The recurrent blooming of *Trichodesmium erythraeum* (Cyanobacteria) in SEAS during March to May months showed the biological indication of oligotrophy (Padmakumar et al., 2010b; Martin et al., 2013). However, the present study has shown enhanced column chl *a* (>10 mg m^{-2}) and PP (>1200 mg C m^{-2} d^{-1}), especially at stations M1 and M2 until the beginning of June (Figure 5-7). More than 80% of the total chl *a* and PP recorded at these stations were found to be derived from nanophytoplankton (Figure 7). By contrast, low levels column chl *a* (<10 mg m^{-2}) and PP (<1000 mg C m^{-2} d^{-1}) recorded at M3 characteristically complemented the oligotrophic condition of SEAS (Bhattathiri et al., 1996; Jyothibabu et al., 2010). The spatial distribution of phytoplankton *characterizing species* (mostly >20 µm) during this season exhibited a noticeable predominance of diatoms and dinoflagellates, despite the low abundance (Figures 8 and 9). The occurrence of similar *characterizing species,* comprised mainly dinoflagellates *(Tripos furca* and *Dinophysis caudata)* at M1 and M2 showed the biological indication of nutrient depletion. Dinoflagellates mostly prefer to grow in nutrient-depleted coastal waters because of the high competition of diatoms in nutrient-rich waters (Menzel et al., 1963; Cushing, 1989). The drastic decline in picophytoplankton chl *a* and PP evident during this period signifies its less competency with larger size groups in utilizing inorganic nutrients (Calvo-Díaz et al., 2006). In temperate regions, nanophytoplankton community grows actively in NH_4^+ rich coastal waters, as they are capable of faster assimilation of NH_4^+ than NO_3^- and NO_2^- (Kuvaldina et al., 2010; Lips and Lips, 2010). The HPLC derived pigment data (unpublished) of the present study apparently revealed the predominance of fucoxanthin and peridinin (biomarkers of diatoms and dinoflagellates, respectively) over other marker pigments during this period. Therefore, the substantial increase in nanophytoplankton chl *a* and PP recorded at M1 and M2 during the Pr.SWM period could be derived from the small-sized diatoms and dinoflagellates, which were unable to identify microscopically because of their small cell size.

The noticeable increase in phytoplankton chl *a* and PP observed during the peak SWM period (August to September) can be linked to the influence of coastal upwelling (Silas, 1984; Jyothibabu et al., 2018a). However, the observed chl *a* and PP from the study region, especially during the onset (June) and peak SWM (July/August) months, did not complement the corresponding nutrient levels or vice versa because of the time lag in the stabilization and relaxation phases of upwelling process (Lips

and Lips, 2010). Previous studies have documented an exceptionally high phytoplankton chl *a* all along the nearshore waters of SEAS (Habeebrehman et al., 2008; Jyothibabu et al., 2010), including the Alappuzha mud bank region (Silas, 1984; Karnan et al., 2017; Jyothibabu et al., 2018a) during the SWM period as a result of the upwelling induced nutrient enrichments (Bhattathiri et al., 1996; Gireeshkumar et al., 2017). Karnan et al, (2017) have reported a tremendous increase in chl *a* in the AMB region found to be derived from large diatoms (>100 µm), such as *Fragilaria* sp. and *Coscinodiscus* sp. However, such results were not perceived in the present study because of the prevalence of exceptionally high nanophytoplankton growth.

During the Pt.SWM period, the prevalence of drastic decrease in chl *a* and PP (both surface and column) evident at all three stations, complemented the prevailing warm nutrient-depleted waters (Figures 5 and 6). The relative increase in nanophytoplankton chl *a* and PP (low levels as compared to SWM) further reveals that this region is still favouring the growth of this particular phytoplankton community. The occurrence of nutrient-depleted waters, particularly NO_3^- (<1µM) and PO_4 (<0.5 µM) as a result of the overutilization of the preceding large-scale phytoplankton growth, maybe the potential cause for the decreased growth of large phytoplankton. In the meantime, the substantial decrease in picophytoplankton chl *a* (<0.1 mg m^{-3}) and PP (<10 mg C m^{-3} d^{-1}) evident during this period indicates the incompetency in nutrient utilization of this particular phytoplankton community than the nanophytoplankton. These results thus contradict the prevailing understanding of picophytoplankton community in the tropical and subtropical coastal waters, wherein they have been recognized as the predominant contributors of marine primary productivity during the oligotrophic periods (Agustí and Llabrés, 2007; Matsumoto et al., 2016).

The RDA analysis indicates the significant influence of NH_4^+ and SiO_4 on the substantial growth of nanophytoplankton throughout the study region, irrespective of seasons (Figure 10a). The widespread increase in NH_4^+ and SiO_4 levels detected in the surface waters substantiates the RDA analytical results (Figure 4). As mentioned in the previous sections, small-sized phytoplankton (<20 µm) usually exhibit faster growth response to the upwelled waters enriched with NH_4^+ (Kuvaldina et al., 2010; Lips and Lips, 2010). Therefore, the present study also reinforces the influence of NH_4^+ on nanophytoplankton growth in coastal waters. Furthermore, distinctively low NO_3^-:PO_4 ratios (<3) prevalent in the overall surface waters of the study region indicated the NO_3^- depleted condition (Table 1). Perhaps, this NO_3^- deficiency in the surface waters could be one of the potential causes of low microphytoplankton growth, even though the water column was enriched with other macronutrients (Figure 4). The substantial contribution of NH_4^+ to the total DIN pool (>80 %), particularly evident in shallow stations (M1 and M2), confirms the profound influence of NH_4^+ on the exceptional growth

and biomass accumulation of nanophytoplankton community. However, according to previous reports, the near shore waters of Alappuzha sustained high NO_3^- levels, particularly during the SWM period (2014) as a result of the intense upwelling, instead of NH_4^+ (Gireesh kumar et al., 2017; Dayana et al., 2019).

Although the present study has revealed larger phytoplankton (diatoms and dinoflagellates) as the major *characterizing species* (SIMPER analysis), its numerical abundance was consistently low in surface waters compared to the corresponding chl *a* levels (Figure 9). Therefore, the observed positive correlation between the *characterizing species* and environmental parameters (NH_4^+, PO_4^{3-}, SiO_4, NO_3^-, PAR, salinity and DO) did not have much relevance (Figure 10a). Regarding PAR, the whole study region remained invariably high levels (>200 µ mole photon m^{-2} d^{-1}) in surface layers, in spite of a marked decrease (<200 µ mole photon m^{-2} d^{-1}) noticed during the onset of SWM (June). Normally, pico-and nanophytoplankton photosynthesis saturates at ~20 µ mole photon $m^{-2}s^{-1}$ in coastal waters, whereas the microphytoplankton requires 100 to 150 µ mole photon $m^{-2}s^{-1}$ for photosynthesis saturation (Anderson et al., 1994; Paczkowska et al., 2020). The PAR in the study region thus indicates the supersaturation levels, even in the mud bank region, irrespective of seasons, and hence, optimum growth of all phytoplankton size groups could be possible in the study region without having any light limitation.

5. Conclusion

In conclusion, this study shows that phytoplankton size structure and allied chl *a* biomass and primary production in the Alappuzha near shore waters (including mud bank region) were governed mainly by inorganic nutrients. The remarkable increase in water column NH_4^+ and moderate SiO_4 and PO_4^{3-} levels prevailed in the study region might have caused a considerable increase in nanophytoplankton growth regardless of seasons. Even though the mud bank region (M2) sustained relatively high water column turbidity during the peak SWM period (July-August), that turbidity level was insufficient to limit the water column PAR required for the phytoplankton growth. Exceptionally high chl *a* and PP recorded at M2 during the upwelling relaxation phase (late SWM period) was apparently associated with the prevailing nutrient enrichments, enabled by the co-existing coastal upwelling and mud bank formation. By contrast, a profound decrease in chl *a* and PP observed at M1 and M2 (during the onset of SWM) and at M3 (during Pr.SWM) indicated the prevalence of oligotrophic condition as a result of the NO_3^- deficiency. The present study, therefore, infers that inorganic nutrient levels were the critical influencing factors of the overall phytoplankton growth in the Alappuzha near shore waters regardless of seasons. Still, further high-resolution measurements on nanophytoplankton community composition (specifically flowcytometry based) are needed to prove

the consistent predominance of this small-sized phytoplankton community in the Alappuzha near shore waters.

Acknowledgments

Authors thank the Director, CSIR-National Institute of Oceanography (NIO), Goa and Scientist-in-Charge, NIO-Regional Centre, Kochi, for providing sufficient financial assistance and support to carry out the field observations and sampling in connection with Alappuzha Mud bank Process studies (AMPS)-II.This is NIO contribution number--.

References

Agustí, S., Llabrés, M., 2007. Solar radiation-induced mortality of marine pico-phytoplankton in the oligotrophic ocean. Photochem. Photobiol. 83(4), 793–801. https://doi.org/10.1111/j.1751-1097.2007.00144.x.

Anabalón, V., Morales, C.E., Escribano, H.R., Varas, M.A., 2007. The contribution of nano- and micro-planktonic assemblages in the surface layer (0–30 m) under different hydrographic conditions in the upwelling area off Concepción, central Chile. Prog. Oceanogr. 75, 396–414.

Andersson, A., Haecky, P., Hagström, A., 1994. Effect of temperature and light on the growth of micro- nano- and picoplankton: impact on algal succession. Mar. Biol. 120, 511–520. https://doi: 10.1007/bf00350071.

Azam, F., Fenchel, T., Field, J.G., Gray, J.S., Meyer-Reil, L.A., Thingstad, F., 1983. The ecological role of water-column microbes in the sea. Mar. Ecol. Prog. Ser. 10, 257–263.

Balachandran, K.K., 2004. Does subterranean flow initiate mud banks off the southwest coast of India? Estuar. Coast. Shelf Sci. 59, 589–598.

Banse, K., 1959. On upwelling and bottom-trawling off the southwest coast of India. J. Mar. Biol. Assoc. India 1, 33–49.

Bhattathiri, P.M.A., Pant, A., Sawant, S.S., Gauns, M., Matondkar, S.G.P., Mohanraju, R., 1996. Phytoplankton production and chlorophyll distribution in the eastern and central Arabian Sea in 1994-1995. Curr. Sci. 71, 857- 862.

Bristow, R.C., 1938. History of Mudbanks. Cochin Govt. Press Vol I and II.

Calvo-Díaz, A., Morán, X.A.G., 2006. Seasonal dynamics of picoplankton in shelf waters of the southern Bay of Biscay. Aquat. Microb. Ecol. 42:159–74.

Clarke, K.R., Gorley, R.N., 2015. PRIMER v7: User Manual/Tutorial. PRIMER-E, Plymouth.

Damodaran, R., 1972. Meiobenthos of the mudbanks of Kerala coast. Proceedings of the Indian Academy of Science (Sect. B), 288–297 pp.

Damodaran, R., 1973. Studies on the benthos of the mudbank regions of Kerala coast. Bulletin Department of Marine Science. University of Cochin, 6 pp.

Dayana, M., Gireeshkumar, T. R., Udayakrishnan, P. B., Muraleedharan, K. R., Madhu, N.V., Nair, M., Revichandran, C., Balachandran, K. K., 2019. Inter-annual variations in the hydrochemistry of Alappuzha mud banks, southwest coast of India. Cont. Shelf Res. 177, 42- 49.

Estrada, M., Delgado, M., Blasco, D., Latasa, M., Cabello, A.M., Benítez-Barrios, V., Fraile-Nuez, E., Mozetič, P., Vidal, M., 2016. Phytoplankton across tropical and subtropical regions of the Atlantic, Indian and Pacific oceans. *PLoS One, 11*(3). https://doi:10.1371/journal.pone.0151699.

Fenchel, T., 1988. Marine plankton food chains. *Annu. Rev. Ecol. Syst. 19*(1), 19-38 pp.

Figueiras, F.G., Labarta, U., Fernández Reiriz, M,J., 2002. Coastal upwelling, primary production and mussel growth in the Rías Baixas of Galicia. Hydrobiologia 484:121–131.

Gireeshkumar, T.R., Mathew, D., Pratihary, A.K., Naik, H., Narvekar, K.U., Araujo, J., Naqvi, S.W.A., 2017. Influence of upwelling induced nearshore hypoxia on the Alappuzha mud banks, South West Coast of India. Cont. Shelf Res. 139, 1–8.

Goldman, J.C., McCarthy, J.J., Peavey, D.G., 1979. Growth rate influence on the chemical composition of phytoplankton in oceanic waters. *Nature*, *279*(5710), 210-215.

Gopinathan, C.K., Qasim, S.Z., 1974. Mud banks of Kerala – their formation and characteristics. Indian J. Mar. Sci. 3, 105–114.

Grasshoff, K., Ehrhardt, M., Kremling, K., 1983. Methods of Sea Water Analysis, second ed. VerlagChemie, Weinhein.

Habeebrehman, H., Prabhakaran, M.P., Jacob, J., Sabu, P., Jayalakshmi, K.J., Achuthankutty, C.T., Revichandran, C., 2008. Variability in biological responses influenced by upwelling events in the Eastern Arabian Sea. J. Mar. Syst. 74, 545–560.

Hareesh Kumar, P. V., M. Joshi, K. V. Sanilkumar, P. Anand, K. Anilkumar, A. D. Rao., C. V. K. Prasada Rao. 2009. "Growth and Decay of Arabian Sea Mini Warm Pool during May 2000 – Observations and Simulations." Deep-Sea Res. 56: 528–540.

Jagadeesan, L., Jyothibabu, R., Arunpandi, N., Karnan, C., Balachandran, K.K., 2017. Dominance of coastal upwelling over Mud Bank in shaping the mesozooplankton along the southwest coast of India during the Southwest Monsoon. Prog. Oceanogr. 156, 252–275.

Jyothibabu, R., Balachandran, K.K., Jagadeesan, L., Karnan, C., Arunpandi, N., Naqvi, S.W.A., Pandiyarajan, R.S., 2018a. Mud Banks along the southwest coast of India are not too muddy for plankton. Sci. Rep. 8 (1), 1–13.

Jyothibabu, R., Devi, C.R.A., Madhu, N.V., Sabu, P., Jayalakshmy, K.V., Jacob, J., Habeebrehman, H., Prabhakaran, M.P., Balasubramanian, T., Nair, K.K.C., 2008. The response of microzooplankton (20–200 μm) to coastal upwelling and summer stratification in the south-eastern Arabian Sea. Cont. Shelf Res. 28, 653–671.

Jyothibabu, R., Madhu, N.V., Habeebrehman, H., Jayalakshmy, K.V., Nair, K.K.C., Achuthankutty, C.T., 2010. Re-evaluation of 'paradox of mesozooplankton' in the eastern Arabian Sea based on ship and satellite observations. J. Mar. Syst. 81, 235–251.

Jyothibabu, R., Pandi, A., Karnan, C., Jagadeesan, L., Manojkumar, T.M., Balachandran, K.K., Naqvi, S.W.A., 2018b. Fragilariopsis sp. bloom causes yellowish-brown waters off Alappuzha, south-central Kerala coast, India, during the mud bank-upwelling phase. Curr. Sci.115 (1),152-159.

Karnan, C., Jyothibabu, R., Arunpandi, N., Jagadeesan, L., Muraleedharan, K.R., Pratihari, A.K., Naqvi, S.W.A., 2017. Discriminating the biophysical impacts of coastal upwelling and mud banks along the southwest coast of India. J. Mar. Syst. 172, 24–42.

Kurup, P.G., 1972. Littoral currents in relations to the mud bank formations along the coast of Kerala, Mahasagar. 5(3), 158-162.

Kuvaldina,N., Lips,I., Lips,U., Liblik,T.,2010. The influence of a coastal upwelling event on chlorophyll a and nutrient dynamics in the surface layer of the Gulf of Finland, Baltic Sea. Hydrobiologia. 639, 221–230.

Lassiter, A.M., Wilkerson, F.P., Dugdale, R.C., Hogue, V.E., 2006. Phytoplankton assemblages in the CoOP-WEST coastal upwelling area. Deep-Sea Res. Part II 53, 3063–3077.

Lips, I., Lips, U., 2010. Phytoplankton dynamics affected by the coastal upwelling events in the Gulf of Finland in July-August 2006. J. Plank. Res. 32 (9), 1269-1282.

Madhu, N.V., 2005. Seasonal studies of primary production and associated environmental parameters in the Indian EEZ. Ph.D. Thesis. Cochin University of Science and Technology, Cochin, India.

Madhu, N.V., Anil, P., Gireeshkumar, T.R., Muraleedharan, K.R., Kiran, K., Vishal, C.R., 2020.Phytoplankton characterisation in the Alappuzha mud banks during the pre-/post phases of a red-tide, *Prorocentrum shikokuense* Hada. Reg. Stud. Mar. Sci. 40. https://doi.org/10.1016/j.rsma.2020.101486.

Madhu, N.V., Martin, G.D., Haridevi, C.K., Nair, M., Balachandran, K.K., Ullas, N., 2017. Differential environmental responses of tropical phytoplankton community in the southwest coast of India. Reg. Stud. Mar. Sci. 16, 21-35.

Madhu, N.V., Reny, P.D., Meenu, Paul., Ullas, N., Resmi, P., 2011. Occurrence of red tide caused by Karenia mikimotoi (toxic dinoflagellate) in the Southwest coast of India. Ind. J. Geo-Mar Sci.40 (6), 821-825.

Mallik, T.K., Mukherji, K.K., Ramachandran, K.K., 1988. Sedimentology of the Kerala mud banks (fluid muds?). Mar. Geol. 80, 99–118.

Malone, T.C., 1980. Size fractionated primary productivity of marine phytoplankton. In: Falkowski PG (ed) Primary productivity in the sea. Plenum, New York, 301–319 pp.

Martin, G.D., Jyothibabu, R., Madhu, N.V., Balachandran, K.K., Nair, M., Muraleedharan, K.R., Arun, P.K., Haridevi, C.K., Revichandran, C., 2013. Impact of eutrophication on the occurrence of Trichodesmium in the Cochin backwaters, the largest estuary along the west coast of India. Environ. Monit. Assess. 185, 1237–1253.

Mathew, K.J., Gopinathan, C.P., Regunathan, A., Rao, D.S., Murty, A.V.S., 1984. Ecology of mudbanks - zooplankton. CMFRI Bull. 31, 35–39.

Matsumoto, K., Abe, O., Fujiki, T., Sukigara, C., Mino, Y. 2016. Primary productivity at the time-series stations in the northwestern Pacific Ocean: Is the subtropical station unproductive? J. Oceanogr. 72(3), 359–371. https://doi.org/10.1007/ s10872-016-0354-4.

Muraleedharan, K.R., Kumar, P.K.D., Kumar, S.P., Srijith, B., John, S., Kumar, K.R.N., 2017. Observed salinity changes in the Alappuzha mud bank, southwest coast of India and its implication to hypothesis of mudbank formation. Cont. Shelf Res. 137, 39–45.

Nair, S.R.S., Devassy, V.P., Madhupratap, M., 1992. Blooms of phytoplankton along the west coast of India associated with nutrient enrichment and the response of zooplankton. Sci. Total Environ. 819–828.

Naqvi, S.W.A., George, M.D., Narvekar, P.V., Jayakumar, D.A., Shailaja, M.S., Sardessai, S., Sarma, V.V.S.S., Shenoy, D.M., Naik, H., Maheswaran, P.A., Krishna Kumari, K., Rajesh, G., Sudhir, A.K., Binu, M.S., 1998. Severe fish mortality associated with 'red tide' observed in the sea off Cochin. Curr. Sci. 75, 543–544.

Paczkowska, J., Brugel, S., Rowe, O., Lefébure,R., Brutemark., A., Agneta Andersson, A., 2020. Response of Coastal Phytoplankton to High Inflows of Terrestrial Matter. Front. Mar. Sci. https://doi.org/10.3389/fmars.2020.00080.

Padmakumar, K,B., Smitha,B.R., Thomas,L.C., Fanimol, C.L., Sreerenjima, G., Menon, N.R., Sanjeevan, V.N., 2010b; Blooms of *Trichodesmium erythraeum* in the South Eastern Arabian Sea during the onset of 2009 summer monsoon. Ocean Sci J. 45(3), 151-157.

Padmakumar, K.B., Sreerenjima, G., Fanimol, C.L., Menon, N.R., Sanjeevan, V.N., 2010a. Preponderance of heterotrophic Noctiluca scintillans during a multi-species diatom bloom along the southwest coast of India. Int. J. Oceans and Oceanogr. 4, 45–53.

Parsons, T.R., Maita, Y., Lalli, C.M., 1984. A Manual of Chemical and Biological Methods for Seawater Analysis. Pergamon Press, Oxford, 173 pp.

Pauly, D., Christensen, V., 1995. Primary production required to sustain global fisheries. Nature, 374, 255–257.

Philip, A.S., C.A. Babu, P.V. Hareeshkumar., 2013. Meteorological aspects of mud bank formation along south west coast of India. Cont. Shelf Res. https://doi.org/10.1016/j.csr.2013. 05.016.

Pomeroy, L.R., 1974. The ocean's food web, a changing paradigm. Bioscience 24, 499–504.

Qasim, S.Z., 2003. Indian Estuaries. Allied Publication Pvt. Ltd., Heriedia Marg, Ballard estate, Mumbai, p. 259.

Ramaiah, N., Paul, J. T., Fernandes, V., Raveendran, T.V., Raveendran. O., Sundar. D., Revichandran, C., Shenoy, D. M., G.M., Kurien, S., Gerson, V. J., Shoji, D. T., Madhu, N. V., Sreekumar, S., Lokabharathi, P. A., Shetye, S. R., 2005. The September 2004 stench off the southern Malabar coast – A consequence of holococcolithophore bloom; Curr. Sci. 88(4) 551–554.

Ramasastry, A.A., Myrland, P., 1959. Distribution of temperature, salinity and density in the Arabian Sea along the South Malabar Coast (South India) during the post-monsoon season. Indian J. Fisheries. 6, 223–255.

Rao,G.D., Kanuri,V.V., Kumaraswami,M., Ezhilarasan,P., Rao,V.D., Sivaji Patra, Dash,S.K., Magesh Peter, Ranga Rao.V., Ramu.K., 2017. Dissolved nutrient dynamics along the southwest coastal waters of India during northeast monsoon: a case study. Chem. Ecol. 33, 3, 229 - 246.

Raven, J.A., 1986. Physiological consequences of the extremely small size of autotrophic organisms in the sea. Can. Bull. Fish. Aquat. Sci. 214:1–70.

Reghunathan, A., Mathew, K.J., Rao, D.S., Gopinathan, C.P., Kurup, N.S., Murty, A.V.S., 1984. Fish and fisheries of the mudbanks. CMFRI Bull. 31, 60–71.

Ryther, J.H and Dunstan,W.M., 1971. Nitrogen, phosphorus, and eutrophication in the coastal marine environment. Science. 171 (3975): 1008-13. ttps://doi:10.1126/science.171.3975.1008.

Sahayak, S., Jyothibabu, R., Jayalakshmi, K.J., Habeebrehman, H., Sabu, P., Prabhakaran, M.P., Jasmine, P., Shaiju, P., Rejomon, G., Thresiamma, J., Nair, K. K.C., 2005. Red tide of Noctiluca miliaris off south of Thiruvananthapuram subsequent to the 'stench event' at the southern Kerala coast. Curr. Sci. 89, 1472 –1473.

Samiksha, S.V., Vethamony, P., Rogers, W.E., Pednekar, P.S., Babu, M.T., Dineshkumar, P.K. 2017. Wave energy dissipation due to mudbanks formed off southwest coast of India. Estuar. Coast. Shelf Sci. 196, 387-398. https://doi.org/10.1016/j.ecss.2017.07.018.

Shangguan, Y., Glibert, P.M., Alexander, J.A., Madden, C. J., Murasko, S., 2017. Nutrients and phytoplankton in semi enclosed lagoon systems in Florida Bay and their responses to changes in flow from Everglades restoration. Limnol. Oceanogr. 62(S1), S327–S347.

Shynu, R., Rao, V.P., Samiksha, S.V., Vethamony, P., Naqvi, S.W.A., Kessarkar, P.M.,Dineshkumar, P.K., 2017. Suspended matter and fluid mud off Alleppey, southwest coast of India. Estuar. Coast. Shelf Sci. 185, 31–43.

Sieburth, J.M., Smetacek, V., Lenz, Jr, 1978. Pelagic ecosystem structure: heterotrophic compartments of the plankton and their relationship to plankton size fractions. Limnol. Oceanogr. 23, 1256–1263.

Silas, E.G., 1984. Mud Banks of Kerala – Karnataka – Need for integrated study. Bull.Central Mar. Fisheries Res. Inst. 31, 1–2.

Smitha, A., Joseph, K.A., Jayaram, C., Balchand, A.N., 2014. Upwelling in the southeastern Arabian Sea as evidenced by Ekman mass transport using wind observations from OCEANSAT–II Scatterometer.

Sommer, U., 2012. Plankton Ecology: Succession in Plankton Communities. Springer Science & Business Media.

Stolte, W., McCollin, T., Noordeloos, A. A. M., Riegman, R., 1994. Effect of nitrogen source on the size distribution within marine phytoplankton populations. J. Exp. Mar. Biol. Ecol. 184, 83–97.

Subrahmanyam, R., 1959. Studies on the phytoplankton of the west coast of India. Proceedings of the Indian Academy of Science, Part I, 508, 113–187 pp.

Tatavarti, R., Narayana, A.C., 2006. Hydrodynamics in a mud bank regime during Nonmonsoon and monsoon seasons. J. Coast. Res. 226, 1463–1473.

Tatavarti, R., Narayana, A.C., Manojkumar, P., Chand, S., 1999. Mud Bank regime off the Kerala coast during monsoon and non-monsoon seasons. J. Earth Syst. Sci. 108, 57–68.

Tomas, C. R., 1997. Identifying Marine Phytoplankton, Academic Press/ Harcourt Brace, San Diego, CA, USA, 858 pp.

Utermöhl, H., 1958. Zur vervolkommung der quantitativen phytoplankton-methodik. Mitt. Int. Ver. Theor. Angew. Limnol. 9, 1–38 (in German).

Verma, U.P., Kurup, P.G., 1969. Formation of Chakara (Mud Bank) in the Kerala coast. Curr. Sci. 38, 559–560.

Vijay, J.G., Madhu, N.V., Jyothibabu, R., Balachandran, K. K., Nair, M., Revichandran, C., 2014. Oscillating environmental responses of the eastern Arabian Sea. Indian J Mar Sci. 43(1), 67-75.

Wilkerson, F.P., Dugdale, R.C., Kudela, R.M. and Chavez, F.P., 2000. Biomass and productivity in Monterey Bay, California: contribution of the large phytoplankton. Deep Sea Res. Part II Top. Stud. Oceanogr. *47*(5-6), 1003-1022.

Figure Captions:-

Figure 1 - a) Map of the study area and sampling locations in the Alappuzha near shore waters (red dots represents sampling stations and brick red shaded zone represents mud bank area); Photographs of the Alappuzha mud bank region during (b) Pr.SWM, (c) SWM and (d) Pt.SWM periods.

Figure 2- Representation (daily average) of wind speed (m s^{-1}) and rainfall (mm d^{-1}) in the Alappuzha coastal region.

Figure 3 - Vertical distribution of temperature (°C), salinity, turbidity (NTU) and PAR (µ mole photon m^{-2} d^{-1}) in the Alappuzha near shore waters.

Figure 4 - Vertical distribution of dissolved oxygen (µM), ammonium (µM), nitrate (µM), phosphate (µM), silicate (µM) in the Alappuzha near shore waters.

Figure 5 - Vertical distribution of biomass (chlorophyll *a* - mg m^{-3}) of various phytoplankton size-groups (micro-, nano- and pico-) in the Alappuzha near shore waters.

Figure 6 - Vertical distribution of primary production rates (mgC m^{-3} d^{-1}) of various phytoplankton size-groups (micro-, nano- and pico-) in the Alappuzha near shore waters.

Figure 7 - Integrated water column chlorophyll *a* (mg m^{-3}) and primary production rates (mg C m^{-2} d^{-1}) of various phytoplankton size-groups (micro-, nano- and pico-) in the Alappuzha near shore waters.

Figure 8 - Distribution of phytoplankton abundance (total, diatoms and dinoflagellates) in the Alappuzha near shore (surface) waters.

Figure 9 - Mean seasonal abundance phytoplankton *characterizing species* (SIMPER based) in the Alappuzha near shore (surface) waters.

Figure 10-RDA correlation triplots showing relationships of major environmental parameters with (a) size-fractionated chlorophyll *a* biomass and primary production, and (b) major *characterising species* in the Alappuzha near shore waters (TS-*Thalassiosira subtilis*, CO-*Coscinodiscus* sp., RH-*Rhizosolenia hebetata*, CH-*Chaetoceros* sp., OD-*Odontella* sp., TM-*Trieres mobiliensis*, PL-*Pleurosigma* sp.,NA-*Navicula* sp., PN-*Pseudo-nitzschia seriata*, PM-*Prorocentrum micans*, DC-*Dinophysis caudata*,TF-*Tripos furca*, GO-*Gonyaulax* sp.,DI-*Diplosalis* sp.,PR-*Protoperidinium* sp.)

Figure 1

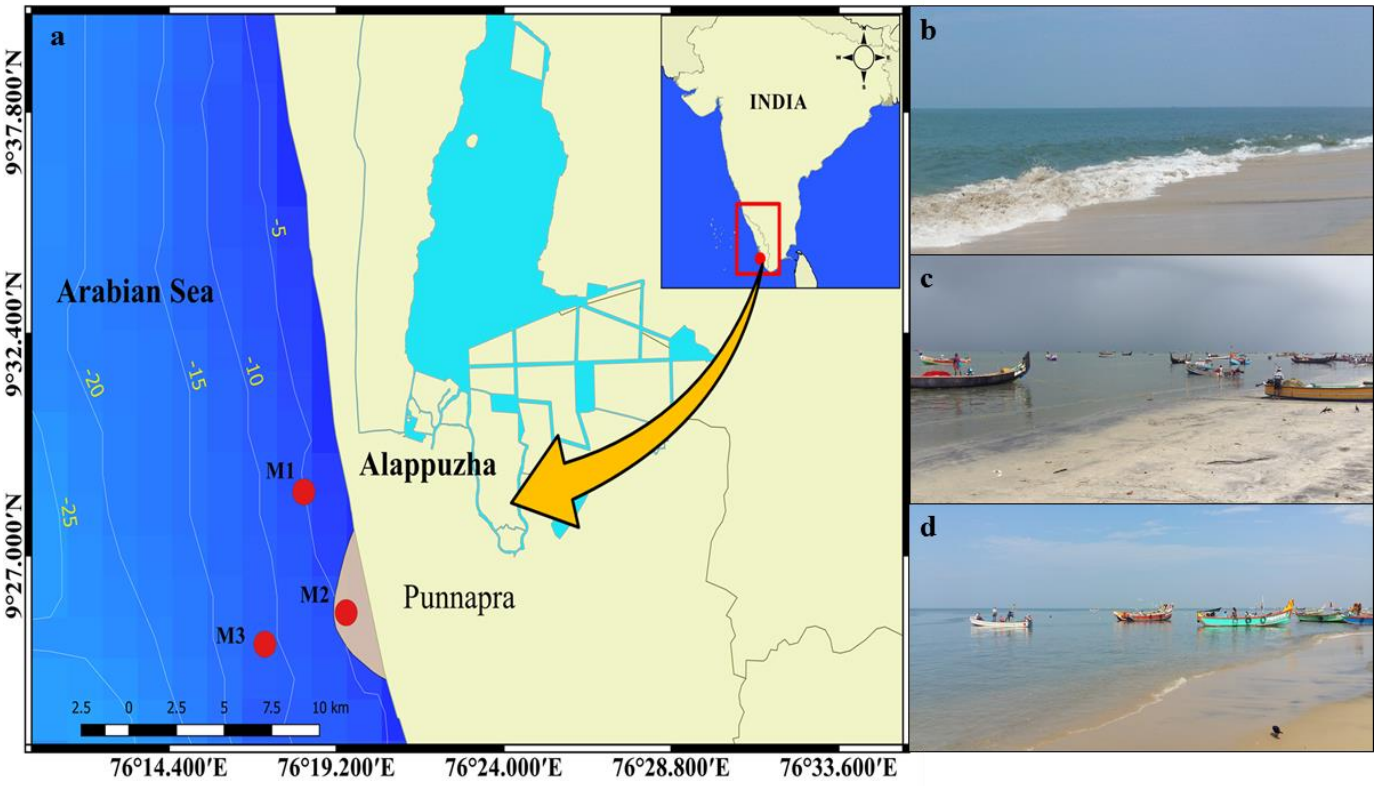
a
b
c
d
INDIA
Arabian Sea
Alappuzha
Punnapra
M1
M2
M3
-5
-10
-15
-20
-25
2.5 0 2.5 5 7.5 10 km
9°37.800′N
9°32.400′N
9°27.000′N
76°14.400′E
76°19.200′E
76°24.000′E
76°28.800′E
76°33.600′E

Figure 2

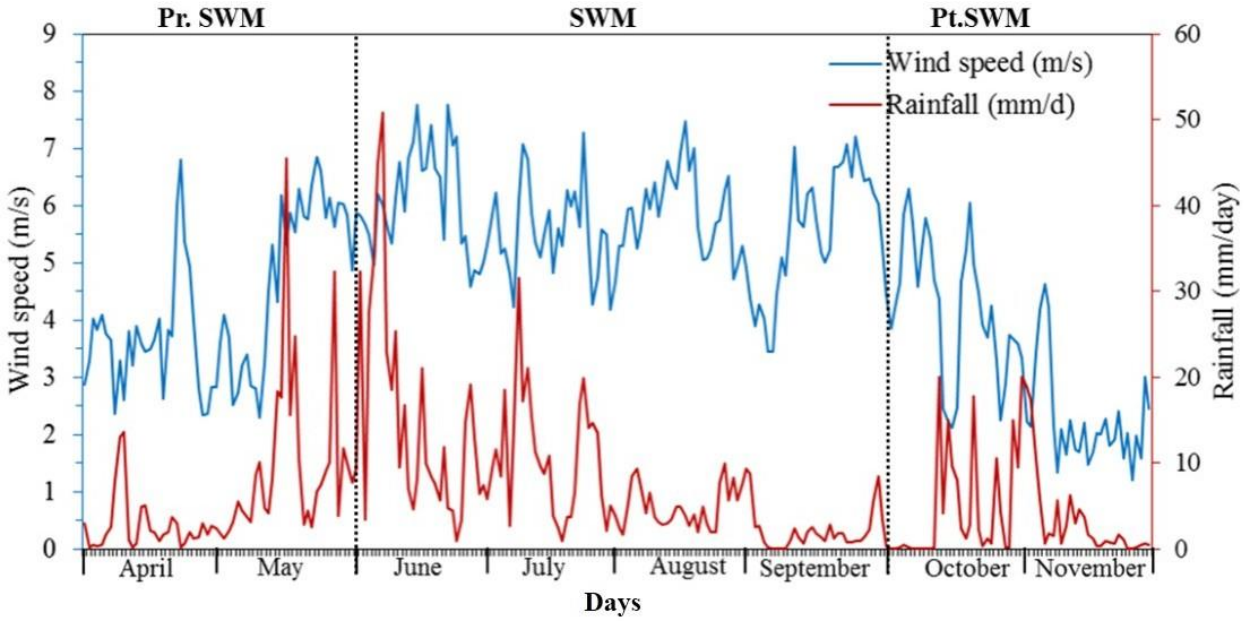
Pr. SWM
SWM
Pt.SWM
Wind speed (m/s)
Rainfall (mm/d)
Wind speed (m/s)
Rainfall (mm/day)
0
1
2
3
4
5
6
7
8
9
0
10
20
30
40
50
60
April
May
June
July
August
September
October
November
Days

Figure 3

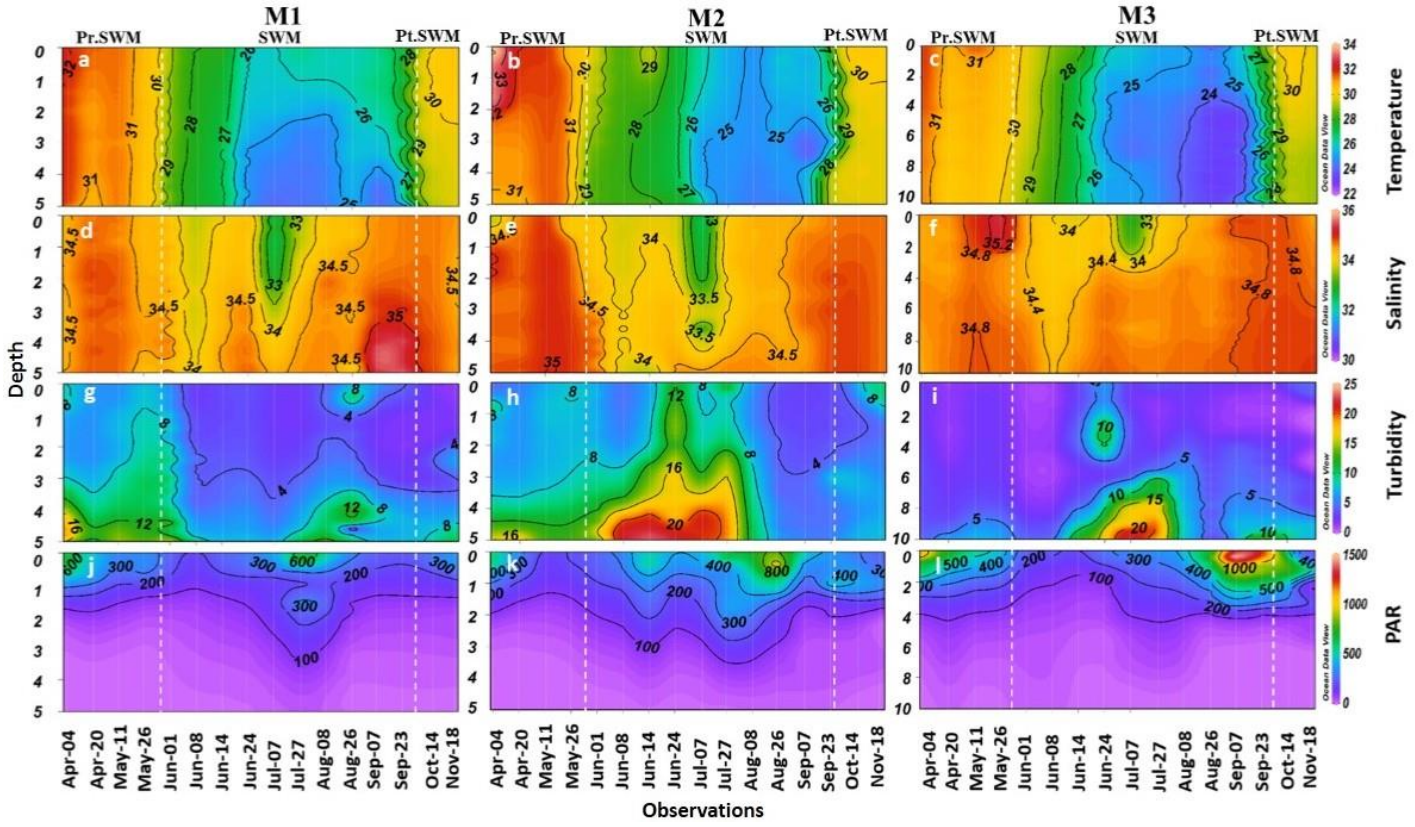
M1
M2
M3
Pr.SWM
SWM
Pt.SWM
Depth
Observations
Temperature
Salinity
Turbidity
PAR
Ocean Data View
Apr-04
Apr-20
May-11
May-26
Jun-01
Jun-08
Jun-14
Jun-24
Jul-07
Jul-27
Aug-08
Aug-26
Sep-07
Sep-23
Oct-14
Nov-18

Figure 4

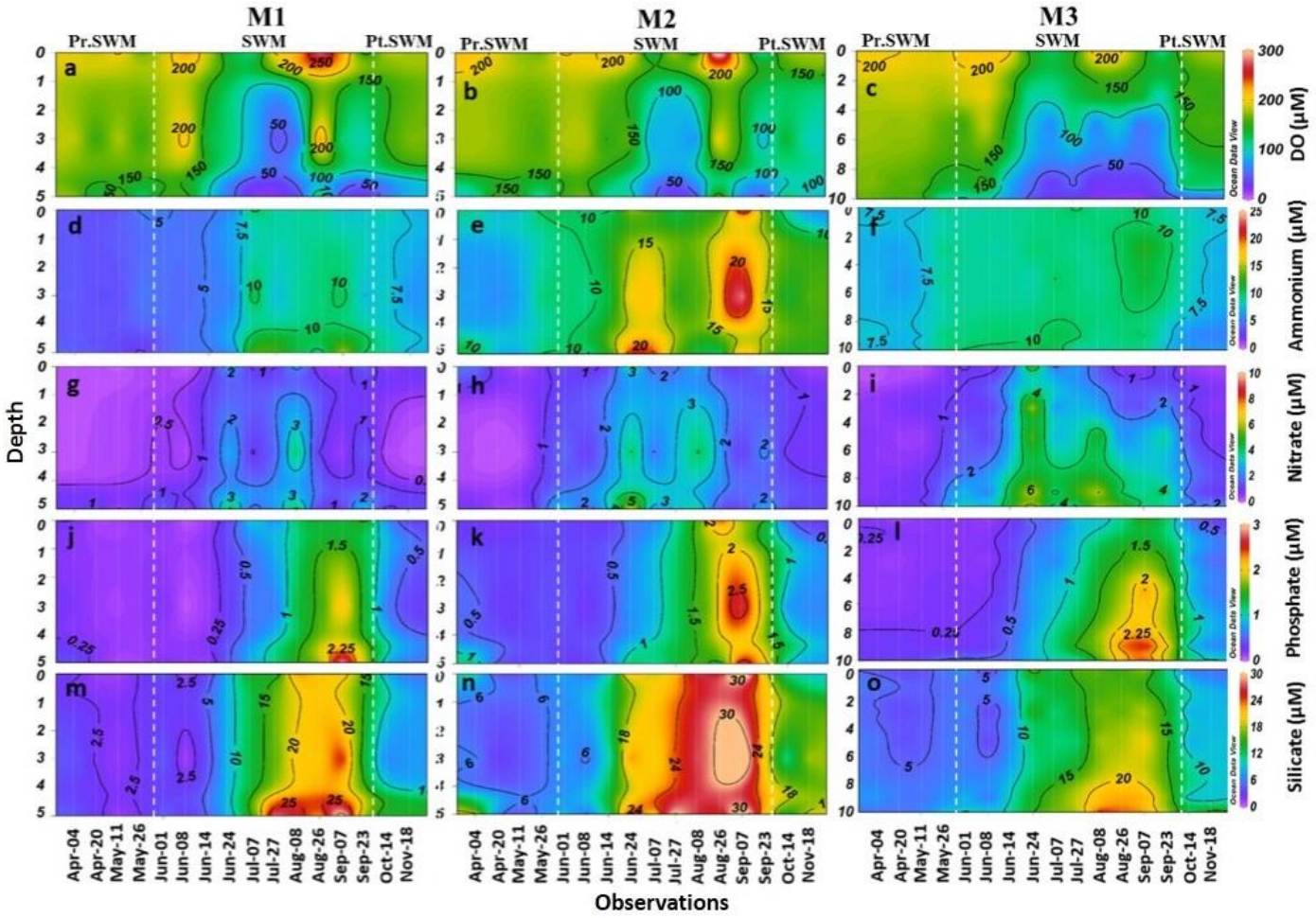
M1
M2
M3
Pr.SWM
SWM
Pt.SWM
Depth
Observations
DO (µM)
Ammonium (µM)
Nitrate (µM)
Phosphate (µM)
Silicate (µM)
Ocean Data View
Apr-04
Apr-20
May-11
May-26
Jun-01
Jun-08
Jun-14
Jun-24
Jul-07
Jul-27
Aug-08
Aug-26
Sep-07
Sep-23
Oct-14
Nov-18

Figure 5

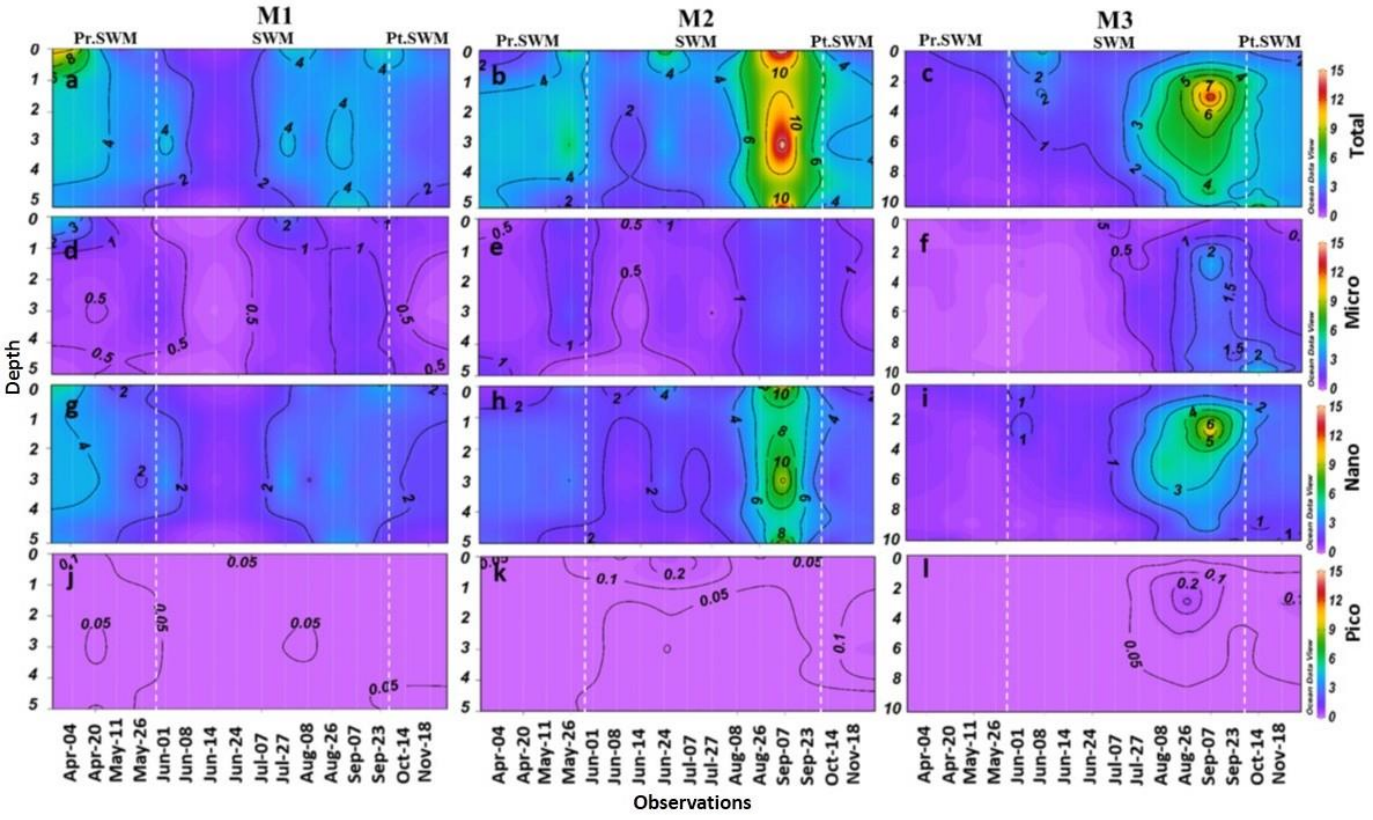
M1
M2
M3
Pr.SWM
SWM
Pt.SWM
Depth
Observations
Total
Micro
Nano
Pico
Apr-04
Apr-20
May-11
May-26
Jun-01
Jun-08
Jun-14
Jun-24
Jul-07
Jul-27
Aug-08
Aug-26
Sep-07
Sep-23
Oct-14
Nov-18

Figure 6

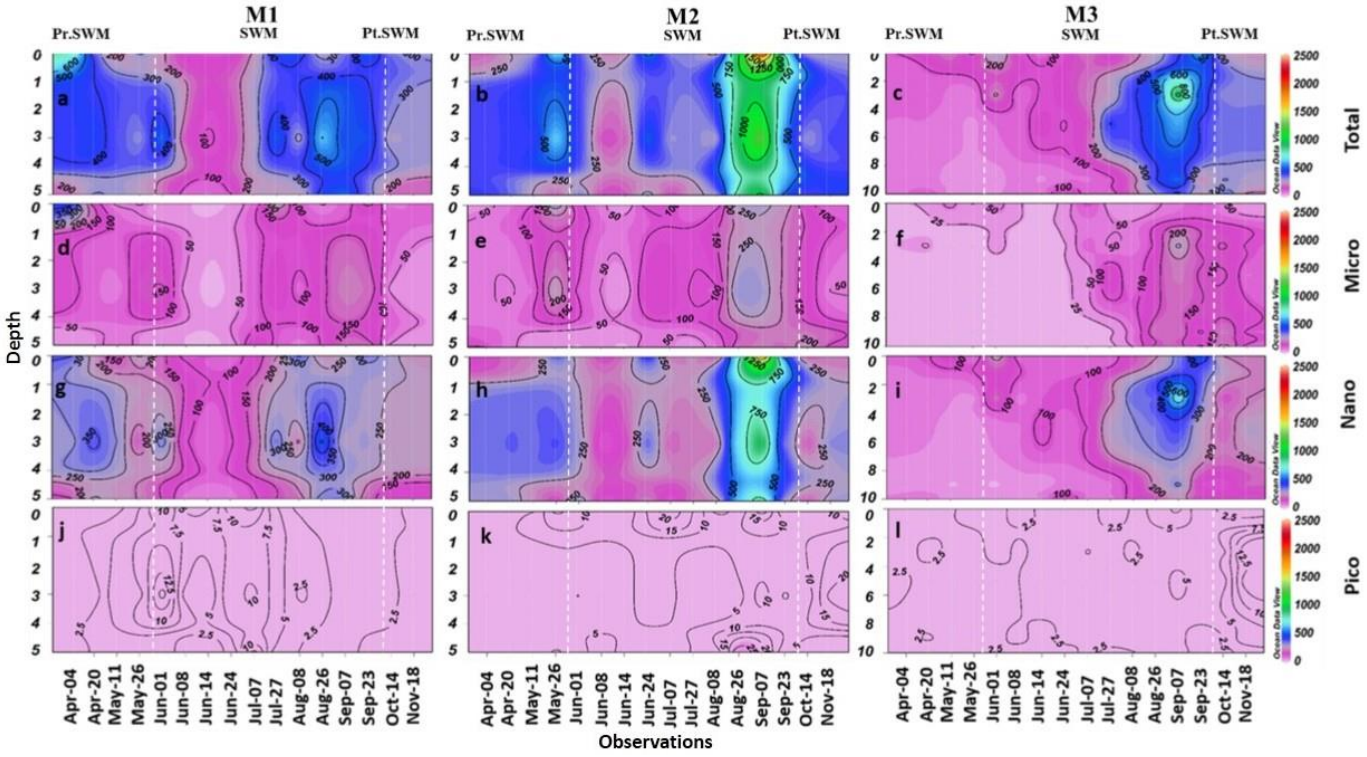
M1
M2
M3
Pr.SWM
SWM
Pt.SWM
Depth
Observations
Total
Micro
Nano
Pico
a
b
c
d
e
f
g
h
i
j
k
l
Apr-04
Apr-20
May-11
May-26
Jun-01
Jun-08
Jun-14
Jun-24
Jul-07
Jul-27
Aug-08
Aug-26
Sep-07
Sep-23
Oct-14
Nov-18

Figure 7

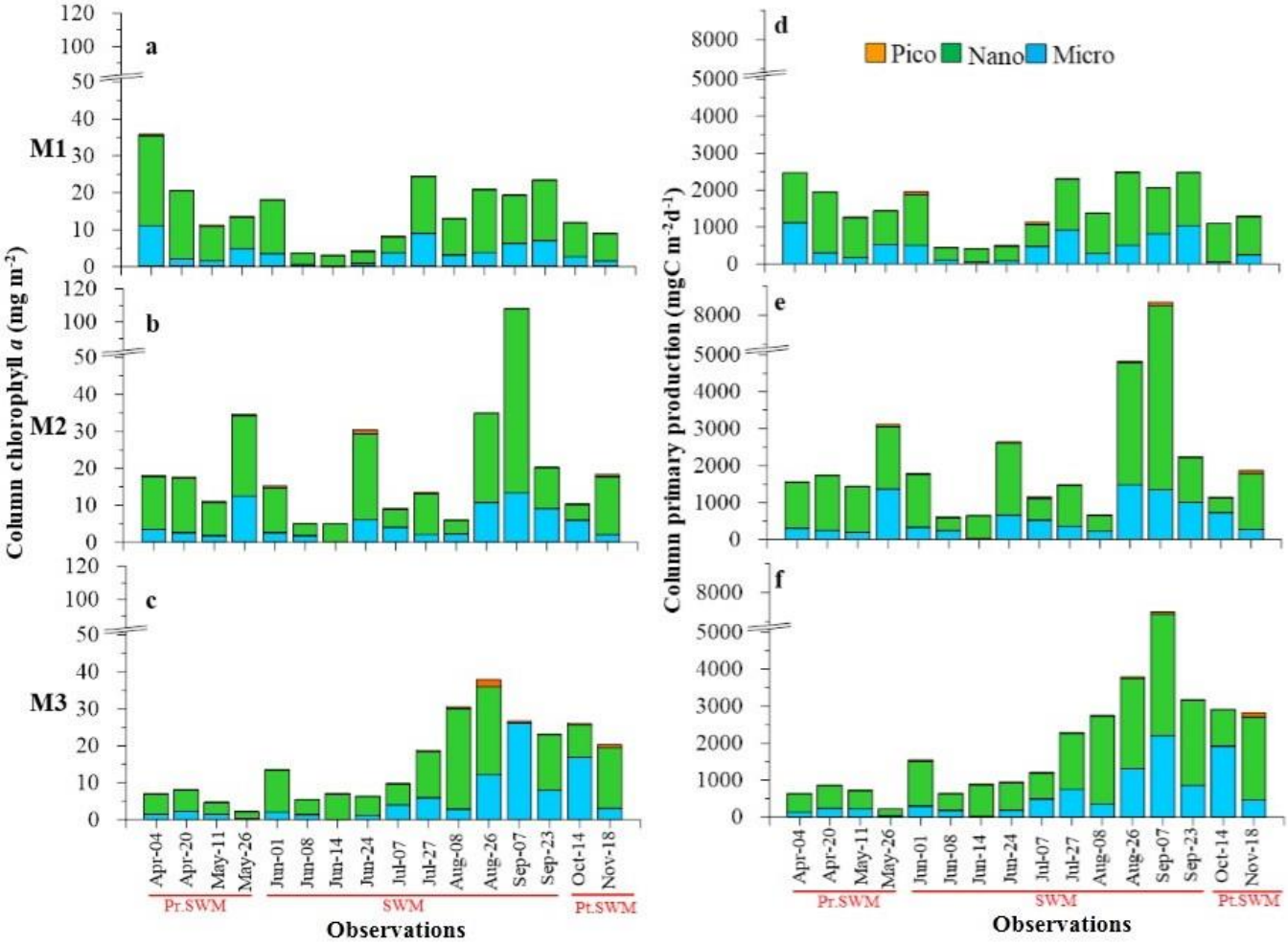
a
b
c
d
e
f
M1
M2
M3
Pico
Nano
Micro
Column chlorophyll a (mg m-2)
Column primary production (mgC m-2d-1)
Apr-04
Apr-20
May-11
May-26
Jun-01
Jun-08
Jun-14
Jun-24
Jul-07
Jul-27
Aug-08
Aug-26
Sep-07
Sep-23
Oct-14
Nov-18
Pr.SWM
SWM
Pt.SWM
Observations

Figure 8

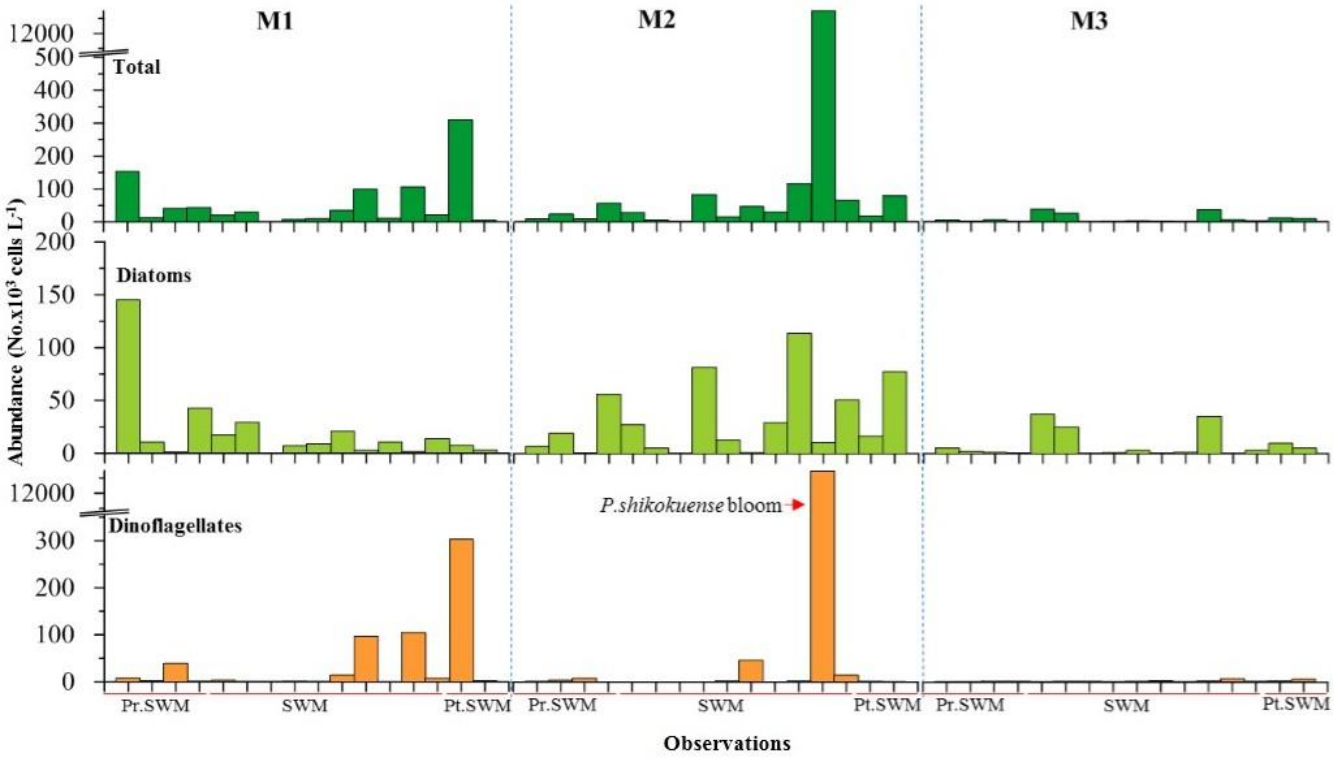
M1
M2
M3
Total
Diatoms
Dinoflagellates
P.shikokuense bloom
Abundance (No.x10³ cells L⁻¹)
Pr.SWM
SWM
Pt.SWM
Observations

Figure 9

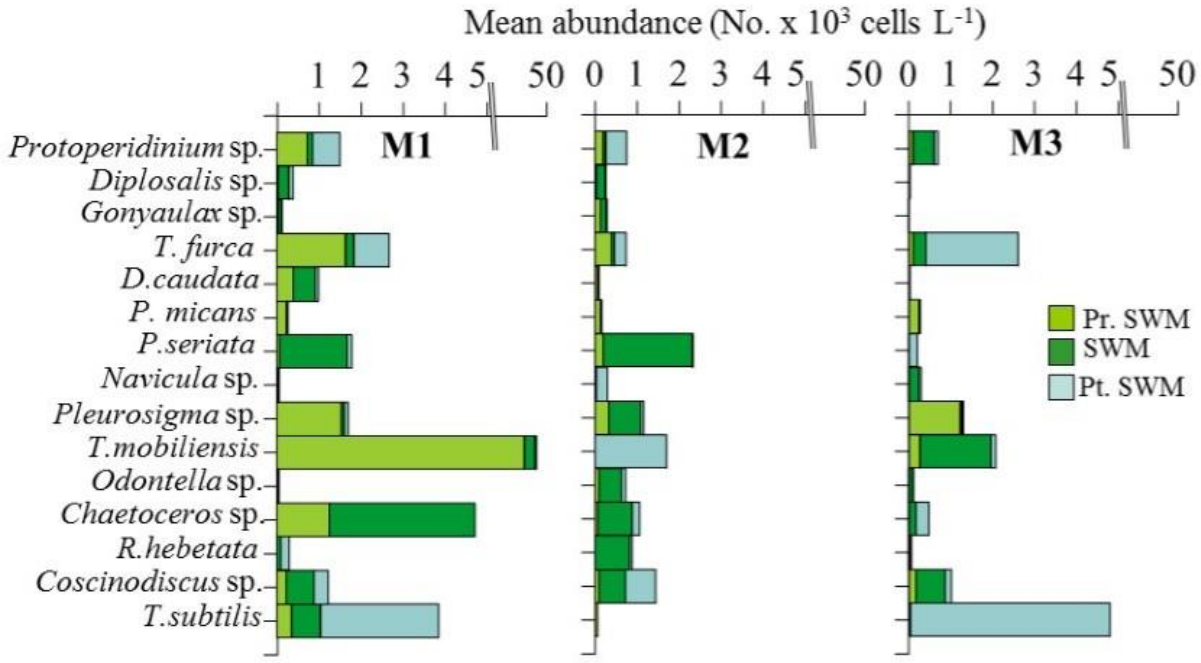
Mean abundance (No. x 10³ cells L⁻¹)
1 2 3 4 5 50 0 1 2 3 4 5 50 0 1 2 3 4 5 50
M1
M2
M3
Protoperidinium sp.
Diplosalis sp.
Gonyaulax sp.
T. furca
D.caudata
P. micans
P.seriata
Navicula sp.
Pleurosigma sp.
T.mobiliensis
Odontella sp.
Chaetoceros sp.
R.hebetata
Coscinodiscus sp.
T.subtilis
Pr. SWM
SWM
Pt. SWM

Figure 10

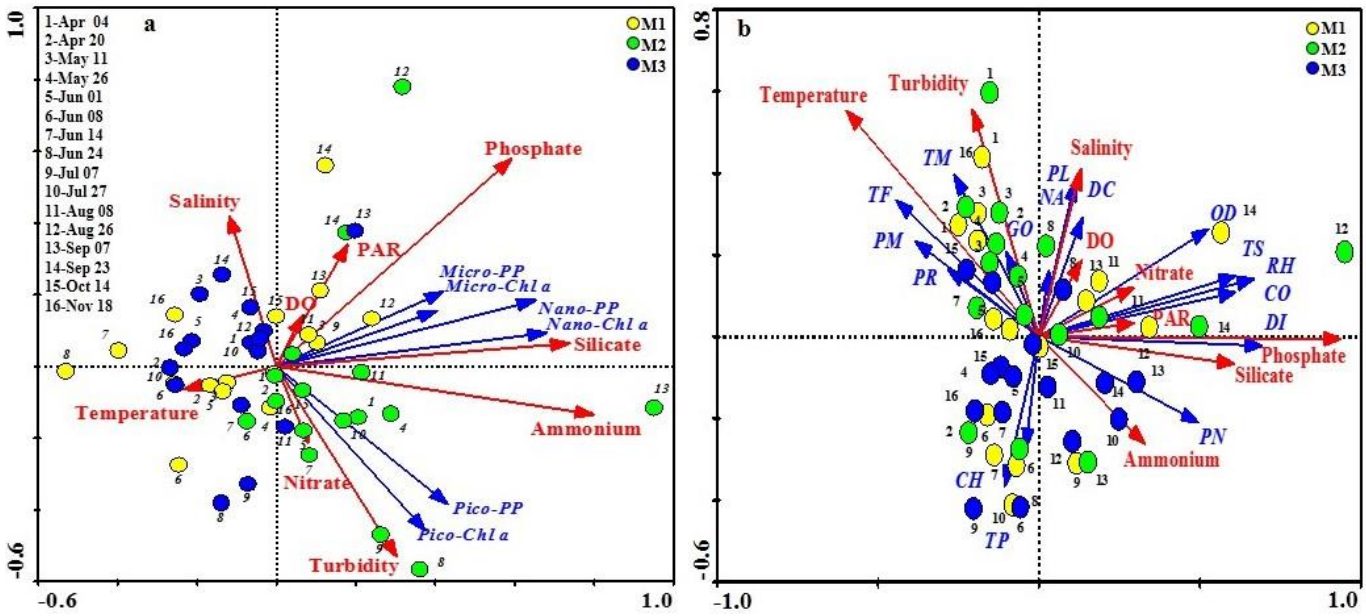
a
1-Apr 04
2-Apr 20
3-May 11
4-May 26
5-Jun 01
6-Jun 08
7-Jun 14
8-Jun 24
9-Jul 07
10-Jul 27
11-Aug 08
12-Aug 26
13-Sep 07
14-Sep 23
15-Oct 14
16-Nov 18
M1
M2
M3
Phosphate
Salinity
PAR
DO
Micro-PP
Micro-Chl a
Nano-PP
Nano-Chl a
Silicate
Temperature
Ammonium
Nitrate
Pico-PP
Pico-Chl a
Turbidity
1.0
-0.6
-0.6
1.0
b
M1
M2
M3
Temperature
Turbidity
Salinity
TM
PL
NA
DC
TF
GO
DO
OD
TS
RH
CO
DI
PM
PR
Nitrate
PAR
Phosphate
Silicate
PN
Ammonium
CH
TP
0.8
-0.6
-1.0
1.0

Table captions:-

Table 1 - Seasonal mean of major physico-chemical and phytoplankton parameters in the nearshore (surface) waters of Alappuzha

Parameters	Pr.SWM			SWM			Pt.SWM		
	M1	M2	M3	M1	M2	M3	M1	M2	M3
Temperature (°C)	31.3 ± 0.7	32 ± 1.4	31.4 ± 1.1	26.7 ± 1.2	26.8 ± 1.9	26.3 ± 2.2	30.4 ± 0.2	30.3 ± 0.1	30.2 ± 1
Salinity	34.4 ± 0.1	34.4 ± 0.6	34.9 ± 0.6	34.1 ± 0.9	34 ± 0.8	34.2 ± 0.9	34.6 ± 0.1	34.7 ± 0.01	34.7 ± 0.3
Turbidity (NTU)	8.4 ± 2.5	5.9 ± 4.1	1.9 ± 1.3	4.1 ± 4.5	7 ± 7.2	2.7 ± 2.1	1.3 ± 0.1	5.6 ± 6	2.6 ± 2.3
PAR (µ mole photon $m^{-2}d^{-1}$)	442.5± 194.5	392.2 ± 393.2	783.5 ± 467.3	311.1 ± 232.9	646.2 ± 454.7	501.1 ± 517.2	345.1 ± 27.7	385.7 ± 179.8	411.8 ± 296.3
DO (µM)	186.6 ± 29	186.7 ± 28.2	196 ± 9.7	191.3 ± 68.2	185.6 ± 93.9	172.6 ± 55.1	187 ± 11.7	186.5 ± 8.2	183.5 ± 1.3
DIN (µM)	4.3 ± 1.4	10.3 ± 2.8	8.3 ± 2.1	8.7 ± 3	15.3 ± 6.4	11.3 ± 2.7	8.5 ± 1.7	6.7 ± 2.2	8 ± 2.1
Ammonium (µM)	4 ± 1.2	8.7 ± 2.5	8 ± 2.1	7.3 ± 2.5	13 ± 5.89	9.3 ± 1.2	7.9 ± 2.5	6.3 ±2.2	7.6 ± 2
Nitrite (µM)	0.1 ± 0.1	0.8 ± 1.4	0.1 ± 0.2	0.3 ± 0.4	0.5 ± 0.6	0.3 ±0.2	0.1 ± 0.01	0.2	0.4 ± 0.02
Nitrate (µM)	0.2 ± 0.1	1 ±1.6	0.2 ± 0.1	1.1 ± 1.2	1.8 ± 1.9	1.7 ± 2.3	0.6 ± 0.8	0.2 ± 0.1	0.2 ± 0.2
Phosphate (µM)	0.2 ± 0.1	0.3 ± 0.1	0.2 ± 0.1	0.8 ± 0.7	1.1 ± 0.8	0.8 ± 0.6	0.4 ± 0.2	0.3 ± 0.1	0.2 ± 0.1
Silicate (µM)	2 ± 1.2	6.4 ± 5.1	4.9 ± 2.1	13.2 ± 8.6	19.7 ± 11.9	12.9 ± 6.3	5.8 ± 1.1	8.9 ± 0.2	4.4 ± 1.5
N:P	38.6 ± 25.4	35.5 ± 8.1	51 ± 30.8	20.2 ± 15.6	22.3 ± 13.2	33.4 ± 37.9	26.5 ± 7.7	23 ± 3.7	37.6 ± 12.6
N:Si	2.6 ± 1.1	2.3 ± 1.1	1.9 ± 0.5	1.6 ± 2.4	1 ± 0.6	1.1 ± 0.7	1.5 ± 0.02	0.8 ± 0.3	2 ± 1.1
Si:P	14.8 ± 7.6	18.8 ± 8.6	18.2 ± 5.5	19.9 ± 13	22.6 ± 10	31.8 ± 6.1	26.3 ± 9.3	24.8 ± 12.5	24.5 ± 20.2
Total Chl *a* (mg m^{-3})	5.2 ± 5.4	3.2 ± 3.8	0.9 ± 0.7	2.7 ± 2.2	5.8 ± 6.8	1.9 ± 1.2	2.8 ± 1.2	2 ± 0.1	1.7 ± 0.1
Micro-Chl *a* (mg m^{-3})	1.9 ± 2.9	1.1 ± 1.4	0.2 ± 0.3	0.8 ± 1.3	1.2 ± 1.0	0.5 ± 0.4	0.8 ±0.2	0.7 ± 0.4	0.3 ± 0.3
Nano-Chl *a* (mg m^{-3})	3.3 ± 2.5	2.1 ± 2.5	0.6 ± 0.5	1.8 ± 1.6	4.5 ± 5.9	1 ± 0.8	2.1 ± 1	1.2 ± 0.3	1.4 ± 0.2
Pico-Chl *a* (mg m^{-3})	0.1 ± 0.1	0.1 ± 0.1	0.02 ± 0.01	0.03 ± 0.02	0.1 ± 0.2	0.04 ± 0.01	0.03 ± 0.02	0.1 ± 0.01	0.03 ± 0.01
Total PP (mgC $m^{-3}d^{-1}$)	408.2 ± 358.8	355.8 ± 304.2	109.4 ± 86.3	273.2 ± 175.6	580.3 ±699.5	237.6 ± 190.8	286.3 ± 0.7	231.5 ± 82.6	196.6 ± 23.8
Micro-PP (mgC $m^{-3}d^{-1}$)	161.8 ± 234.5	131 ± 157	26.8 ± 31	80.9 ± 95.8	131.3 ± 108.2	51.0 ± 40.8	50.3 ± 51	77.4 ± 17.1	25.3 ± 14.1
Nano-PP (mgC $m^{-3}d^{-1}$)	244.1 ± 153	217.7 ± 140.5	80.5 ± 57.7	186.6 ± 117.9	437.5 ± 623.3	182.9 ± 163.8	233.4 ± 52.4	146.4 ± 93.3	159.4 ± 38.1
Pico-PP (mgC $m^{-3}d^{-1}$)	2.4 ± 1.3	7.1 ± 8.3	2.2 ± 0.9	5.7 ± 5.8	11.6 ± 10.1	3.6 ± 2.9	2.7 ± 2.1	7.8 ± 6.4	2 ± 0.2
Phytoplankton (No.x10^3 cells L^{-1})	62.6 ± 62.2	24.3 ± 22.6	4 ± 2.4	34.4 ± 37.7	88 ± 145.8	12 ± 15.1	158 ± 215.9	48.4 ± 42.7	10.5 ± 0.7
Diatom (No.x10^3 cells L^{-1})	49.8 ± 65.9	20.7 ± 24.9	2.3 ± 2	11.3 ± 9.3	33.3 ± 38.1	10.7 ± 15.4	5.3 ± 3.1	47.1 ± 43.2	7.5 ± 3.2
Dinoflagellate (No.x10^3 cells L^{-1})	12.8 ± 18.2	3.6 ± 3.4	0.7 ± 0.2	23.1 ± 41.3	54.3 ± 148.5	1.3 ± 1.9	152.7 ± 212.7	1.4 ± 0.5	3 ± 2.5